

TEMPOCONTROL: Temporal Attention Guidance for Text-to-Video Models

Shira Schiber, Ofir Lindenbaum, Idan Schwartz

Bar-Ilan University, Israel

Abstract

Recent advances in generative video models have enabled the creation of high-quality videos based on natural language prompts. However, these models frequently lack fine-grained temporal control, meaning they do not allow users to specify when particular visual elements should appear within a generated sequence. In this work, we introduce TEMPOCONTROL, a method that allows for temporal alignment of visual concepts during inference, without requiring retraining or additional supervision. TEMPOCONTROL utilizes cross-attention maps, a key component of text-to-video diffusion models, to guide the timing of concepts through a novel optimization approach. Our method steers attention using three complementary principles: aligning its temporal shape with a control signal (via correlation), amplifying it where visibility is required (via energy), and maintaining spatial focus (via entropy). TEMPOCONTROL allows precise control over timing while ensuring high video quality and diversity. We demonstrate its effectiveness across various video generation applications, including temporal reordering for single and multiple objects, as well as action and audio-aligned generation.

Code — <https://github.com/Shira-Schiber/TempoControl>
Project Page —

<https://shira-schiber.github.io/TempoControl/>

1 Introduction

Generative video models have improved dramatically, enabling the synthesis of high-quality, temporally coherent videos from natural language descriptions (Singer et al. 2022; Blattmann et al. 2023; Yang et al. 2024; Bar-Tal et al. 2024; Wan et al. 2025). These models have enabled creative applications in animation, design, and virtual content creation by generating visually compelling sequences that align with textual descriptions. However, while current models offer strong spatial consistency and global semantics, they lack fine-grained *temporal control*. Specifically, guiding the model to generate visual elements at specific time points is particularly challenging. This includes making an object appear in the middle of a scene or aligning visual aspects of lighting with the sound of thunder (see Figure 1).

Recent works on generative video modeling have proposed various spatial and motion control mechanisms, including object masking, layout conditioning, or added camera controls (Gupta et al. 2024; Wang et al. 2024b; Feng

et al. 2025; He et al. 2024). In contrast, temporal control has received significantly less attention. Incorporating such control typically requires additional supervision in the form of temporally annotated datasets. Since video data is often scarce, extending annotations to capture temporal variation is expensive and often impractical at scale. Synthetic data could be used; however, generating diverse and temporally accurate video-text pairs, especially for abstract concepts such as movement, is a highly non-trivial challenge.

In this work, we propose a lightweight yet effective inference-time control method, TEMPOCONTROL, which introduces temporal control for generated video. Instead of retraining the generative model, TEMPOCONTROL leverages a property already embedded in these systems: the text-frame cross-attention mechanism.

Cross-attention layers inherently encode strong signals about *which* specific words in the prompt are realized in each generated frame. By directly influencing these attention maps during the denoising process, we can shift the temporal alignment of visual concepts without sacrificing quality or requiring additional data. The approach is data-efficient and preserves both the fidelity and diversity of the original generation process.

Attention control is achieved by carefully steering the latent variables during the diffusion process. At each denoising step, we apply a few stochastic gradient descent iterations (Battash, Wolf, and Lindenbaum 2024) until a satisfactory level of temporal alignment is achieved, notably, without updating model parameters.

To guide temporal alignment, TEMPOCONTROL introduces a novel loss with three complementary components, based on: Pearson correlation, energy, and entropy. The Pearson term encourages the temporal shape of attention to match that of an external control signal, operating on the normalized attention vector to align the presence of a concept with the desired timing. However, since correlation is scale-invariant, it may yield high scores even when attention values are too low to render the object visible. To mitigate this, we incorporate an energy term that directly promotes stronger attention in frames where the temporal signal is high, and suppresses it elsewhere. Additionally, we introduce an entropy regularization term to maintain spatial focus, ensuring that when attention is activated, it remains coherent and not diffusely spread across the frame.

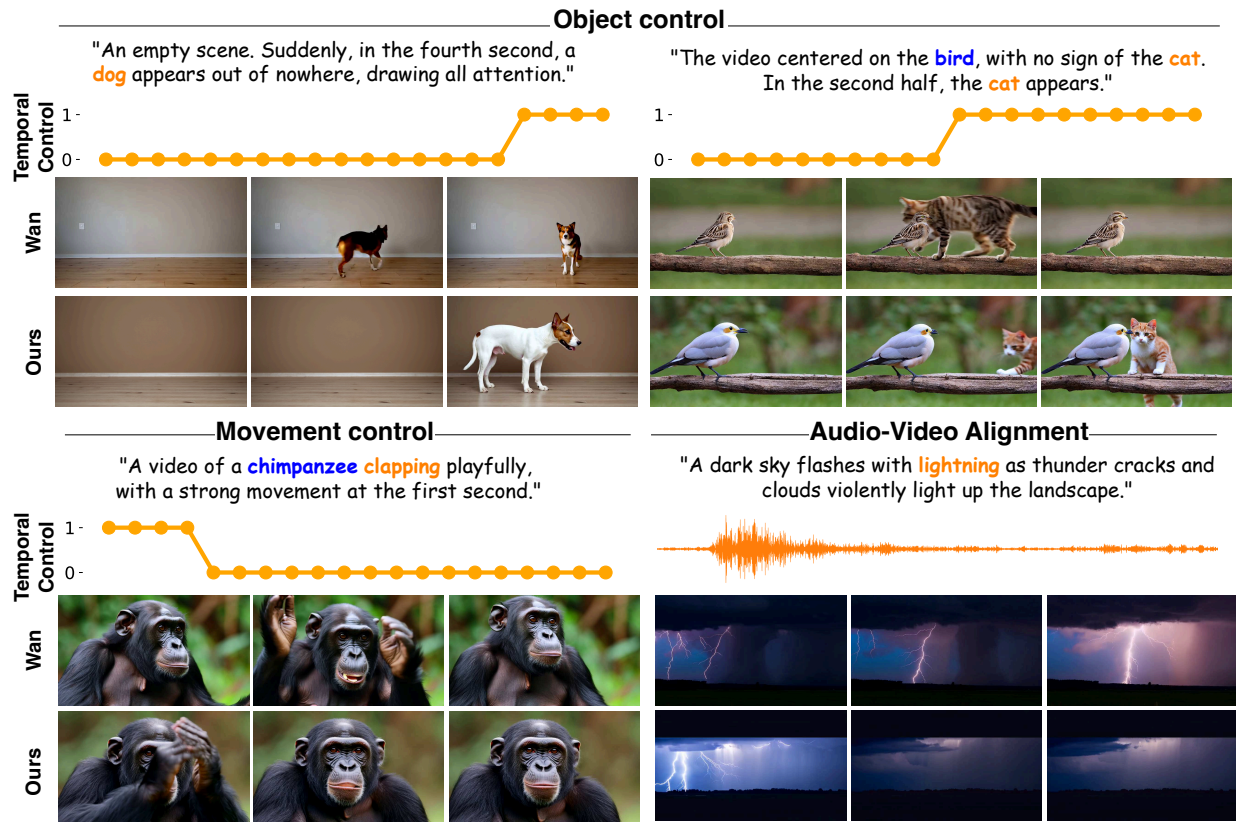


Figure 1: Applications of our inference-time temporal control method (TEMPOCONTROL), which enables multi-object and single-object control, motion control, and audio alignment. Words that are controlled to appear throughout the entire video are shown in blue. Words that appear according to a temporally varying control signal are shown in orange.

Beyond single-object scenarios, as shown in Figure 1, our method generalizes well to multi-object scenes. In such cases, it is important to maintain the visual grounding of non-target entities; we find that preserving one object (e.g., the bird) while selectively manipulating another (e.g., the cat) helps retain the overall scene structure. In addition to nouns, our method can also manipulate verbs (e.g., clapping), effectively modifying the motion depicted in the video. Finally, we explore the potential of aligning external audio cues with video generation. While we focus on simple cases involving a single audio event (e.g., a lightning strike), we observe promising results, suggesting that our approach may naturally extend to zero-shot multimodal control without additional training.

Our contributions are as follows: (i) We propose an inference-time method for temporally controlling the appearance of specific words in text-to-video diffusion models, without requiring model finetuning or additional supervision. (ii) We introduce a suite of losses that operate over spatiotemporal attention to enable fine-grained control over both the timing and intensity of word grounding. (iii) We demonstrate the versatility of our method across various settings, including multi-object control, motion manipulation, and audio-to-video alignment, and introduce a new metric

to evaluate the task of temporal alignment control, which is not covered by existing benchmark suites.

2 Related Work

Motion Control. Fine-grained motion control has been an active area of research. Boximator (Wang et al. 2024b) introduces control by allowing users to specify the spatial locations of a start box and an end box for each object. This control is implemented by fine-tuning a dedicated control module. BlobGEN-Vid (Feng et al. 2025) enhances control by introducing visual primitive-based guidance, such as lines, to enable detailed manipulation of object motion, fine-grained appearance, and smooth object transitions. CameraCtrl (He et al. 2024) addresses controllability by enabling precise camera movement and perspective control. This is accomplished by training a plug-and-play camera pose control module on top of a video diffusion model. Motion Prompting (Geng et al. 2025) enables movement control by incorporating spatio-temporally sparse or dense motion trajectory inputs. However, these approaches require extensive datasets and computational resources for training, substantial user annotations during inference, and notably lack precise control over motion timing or peak movement appearance.

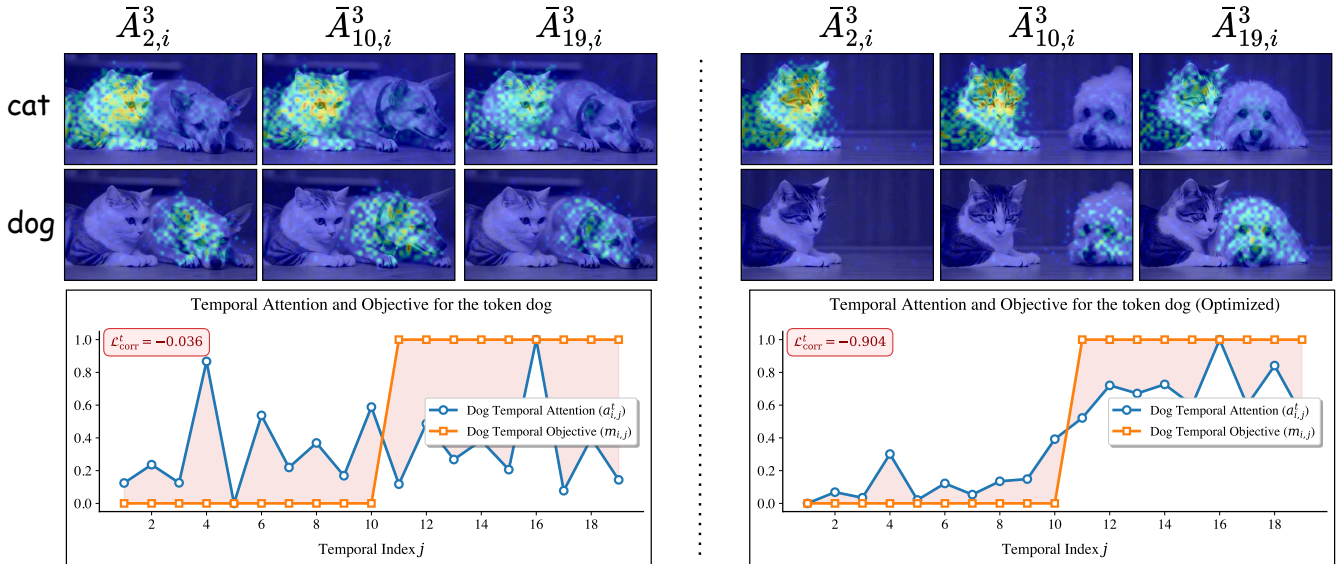


Figure 2: Video generated for the prompt “A cat and a dog.” Before (left) and after optimization (right). Top: Spatial attention maps for the tokens *cat* and *dog* at denoising step $t=3$, shown for frames $j=2, 10, 19$. Attention is overlaid on generated frames. Bottom: temporal attention $a_{i,j}^t$ (blue) vs. target mask $m_{i,j}$ (orange), with Pearson correlation loss shown.

Attention-based Control. Attention-based methods have improved spatial control in text-to-image generation. Prompt-to-Prompt (Hertz et al. 2023) enables word-level edits via cross-attention manipulation, while Attend-and-Excite (Chefer et al. 2023) ensures all mentioned objects are depicted by balancing token attention. Battash et al. (2024) introduced a layout optimization strategy for multi-subject generation in text-to-image diffusion, which constrains cross-attention to improve the spatial separation of objects. Be Yourself (Dahary et al. 2024) uses bounded attention to preserve subject identity and prevent semantic leakage in multi-subject text-to-image generation. Stable Flow (Avrahami et al. 2025) enables training-free image editing by selectively injecting attention features into vital layers of a diffusion transformer. These methods operate on static images, whereas we extend attention-based control to the temporal domain, enabling control over object timing and motion in video generation.

Inference time optimization. Inference-time optimization for text-to-video diffusion has only recently attracted attention. (Li et al. 2025) pre-compute a spatio-temporal sketch and inject plan-consistent noise during sampling to tighten prompt alignment. (Wei et al. 2025) converts a single keyframe into a textured, deformable 3D mesh that is re-rendered at every denoising step to maintain consistency in the garment’s appearance. (Shaulov et al. 2025) derive variance-based optical-flow cues from the model’s latent predictions and add a flow-coherence loss on-the-fly, smoothing motion without retraining. (Lian et al. 2023) let a large language model generate scene graphs and temporal layouts that act as attention masks, improving complex spatio-temporal grounding. While these methods improve fidelity and consistency without necessitating additional train-

ing, none offer explicit, user-defined control over the timing of textual element unfolding.

3 Preliminaries

We build TEMPOCONTROL on top of Wan 2.1 (Wan et al. 2025), a state-of-the-art diffusion model that serves as our backbone for text-to-video generation. Let $v \in \mathbb{R}^{T_v \times H_v \times W_v \times 3}$ represent the input video, where T_v is the number of frames, $H_v \times W_v$ denotes the spatial resolution of each frame, and the final dimension corresponds to the three RGB color channels. The video is first encoded by a 3D causal variational autoencoder into a latent tensor

$$z \in \mathbb{R}^{T' \times H' \times W' \times C}, \quad (1)$$

where T' , H' , and W' denote the temporal and spatial dimensions of the latent representation, which are reduced relative to the input video. Flattening the spatial and temporal dimensions, z is reshaped into a sequence of n_v video tokens, where $n_v = T' \cdot H' \cdot W'$, and each token is a C -dimensional feature vector representing a specific spatiotemporal region of the video.

The text prompt $\mathcal{P} = [p_1, \dots, p_{n_p}]$ is embedded using a pretrained text encoder. For brevity, we refer to tokens as words, although a word may consist of multiple subtokens. All operations described for words are applied to the average of their corresponding subtokens. Video synthesis is then performed as a denoising diffusion process in the latent space, where the model iteratively refines latent variables $\{z_t\}_{t=T}^0$, gradually denoising z_T into z_0 . At each timestep t , a transformer-based network $\text{DiT}(z_t, \mathcal{P}, t)$ predicts the noise in z_t , conditioned on the prompt \mathcal{P} and the timestep t .

3.1 Cross-attention in text-to-video diffusion models

A key challenge in text-to-video generation is ensuring that the synthesized video aligns semantically and temporally with the input prompt. In diffusion-based architectures, this alignment is achieved through cross-attention layers within the transformer blocks at each denoising step t .

During cross-attention, video tokens act as queries that attend to text tokens, which serve as keys and values. This mechanism enables the model to inject contextually relevant linguistic information into each video token representation. The attention weights are computed via scaled dot products between queries and keys, producing a set of attention tensors across layers, $A^t \in \mathbb{R}^{L \times h \times n_v \times n_p}$, where L is the number of cross-attention layers, h is the number of attention heads, n_v is the number of video tokens, and n_p is the number of text tokens. A softmax is applied along the text-token dimension, yielding a probability distribution over prompt words for each video token, per head and per layer.

To obtain a global view of token-level influence, we average attention maps across heads and cross-attention layers, producing an aggregate attention matrix $\bar{A}^t \in \mathbb{R}^{n_v \times n_p}$. This matrix quantifies the influence of each text token on each video token.

The effect of a specific word i is measured by extracting the corresponding column $\bar{A}_i^t \in \mathbb{R}^{n_v}$. The vector \bar{A}_i^t can be reshaped at temporal index j , yielding $\bar{A}_{j,i}^t \in \mathbb{R}^{H' \times W'}$, which represents the spatial influence of word i at temporal position j and denoising step t . Figure 2 illustrates this for the words *cat* and *dog* in the prompt “A cat and a dog.” The attention maps are up-sampled to the frame resolution for visualization.

The attention map captures the spatiotemporal grounding of words in the generated video; TEMPOCONTROL is specifically designed to steer the *temporal* influence of a token. Therefore, we focus on the scalar attention value $\hat{A}_{j,i}^t = \langle \bar{A}_{j,i}^t \rangle_{x,y} \in \mathbb{R}$, where $\langle \cdot \rangle_{x,y}$ denotes summation over the spatial coordinates $x \in [1, H']$ and $y \in [1, W']$. Intuitively, $\hat{A}_{j,i}^t$ measures the influence of word i on the latent representation at temporal position j during the denoising step t .

To summarize the temporal attention pattern of word i at denoising step t , we collect the scalar values across frames into a vector:

$$\hat{a}_i^t = [\hat{A}_{1,i}^t, \hat{A}_{2,i}^t, \dots, \hat{A}_{T',i}^t] \in \mathbb{R}^{T'}. \quad (2)$$

We omit the first frame due to unstable attention values that do not reliably reflect word grounding. This vector serves as the target for our steering method, described in the next section.

4 Method

Given a video v , our goal is to generate an edited version v' such that specific tokens appear according to a temporal condition defined by a weighting mask $m_i = [m_{i,1}, \dots, m_{i,T'}]$, where $m_{i,j} \in [0, 1]$ indicates the desired strength of activation of token p_i at temporal position j (see Figure 2 bottom). In most experiments, we use binary masks (i.e., values of

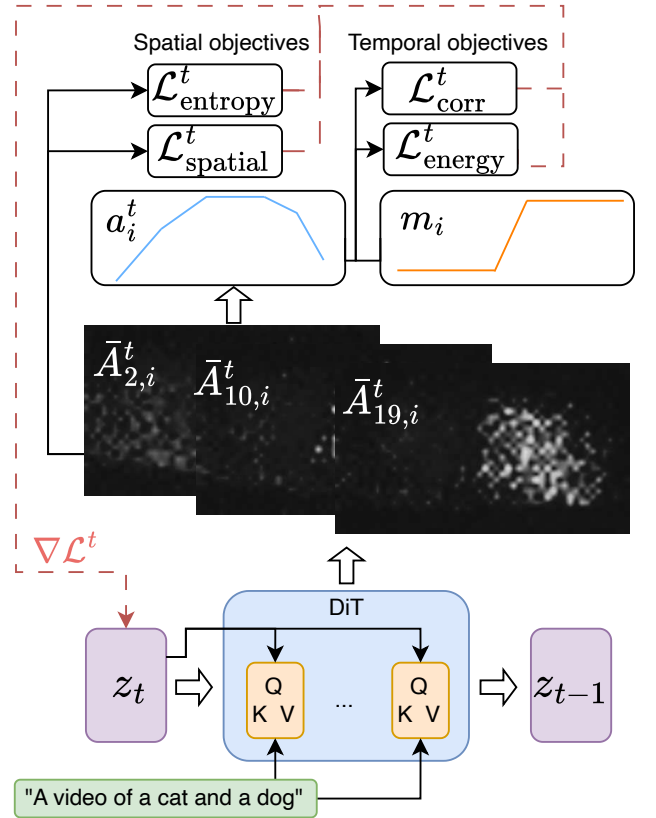


Figure 3: Illustration of TEMPOCONTROL. During a single denoising step t , we extract spatial attention maps $\bar{A}_{j,i}^t$ (for word i at temporal index j), aggregate to a temporal attention signal \hat{a}_i^t , and align it with the target mask vector m_i via temporal and spatial losses. Gradients $\nabla \mathcal{L}$ are used to update the latent code z_t .

zero or one), except for the audio-alignment setting, where the mask reflects sound strength. The main steps of our approach are detailed in the appendix Algorithm 1, illustrated in Figure 3, and discussed below.

We steer the latent representation during the first k denoising steps by performing l gradient update iterations at each step using the AdamW optimizer. For clarity, the update can be expressed as:

$$z'_t = z_t - \alpha \nabla_{z_t} \mathcal{L}^t, \quad (3)$$

where $\alpha \in \mathbb{R}$ is the learning rate and t is the current denoising step. The loss \mathcal{L}^t consists of four components (detailed below): (i) temporal correlation, (ii) energy, (iii) entropy regularization, and (iv) spatial consistency.

Temporal correlation term. The first loss term encourages the temporal attention vector \hat{a}_i^t to match the target mask m_i using the Pearson correlation:

$$\mathcal{L}_{\text{corr}}^t = -\frac{\text{Cov}(m_i, \tilde{a}_i^t)}{\sigma_{m_i} \sigma_{\tilde{a}_i^t}}, \quad (4)$$

where \tilde{a}_i^t is the min-max normalized version of a_i^t , defined as $\tilde{a}_i^t = \frac{a_i^t - \min(a_i^t)}{\max(a_i^t) - \min(a_i^t)}$. Here, $\text{Cov}(\cdot, \cdot)$ denotes empirical

covariance, and σ_{m_i} and $\sigma_{\hat{a}_i^t}$ are the corresponding standard deviations. Note that if m_i has zero variance, such as when encouraging an object to appear throughout the entire video, the correlation term is undefined; in such cases, it is excluded from the loss.

This alignment term adjusts the temporal placement of words in the video but does not affect their overall strength. As a result, words that are initially invisible may remain so. The following loss term is designed to modulate the temporal strength of attention.

Attention energy term. The energy term adjusts the overall magnitude of attention for word token i based on the temporal mask m_i . We use the indicator function $\mathbb{1}_{\{\cdot\}}$, which equals 1 when the condition is true and 0 otherwise. The positive energy encourages attention where the word should be active:

$$\mathcal{L}_{\oplus}^t = \frac{1}{T'} \sum_{j=1}^{T'} \mathbb{1}_{\{m_{i,j} > \tau\}} \cdot a_{i,j}^t. \quad (5)$$

The negative energy penalizes attention where the word should not be visible:

$$\mathcal{L}_{\ominus}^t = \frac{1}{T'} \sum_{j=1}^{T'} \mathbb{1}_{\{m_{i,j} \leq \tau\}} \cdot a_{i,j}^t. \quad (6)$$

The final energy loss is defined as the net difference:

$$\mathcal{L}_{\text{energy}}^t = \mathcal{L}_{\ominus}^t - \mathcal{L}_{\oplus}^t. \quad (7)$$

Here, $\tau \in [0, 1]$ is a threshold that determines whether a given time index is considered active for token p_i . While m_i is often binary (i.e., 0 or 1), it may also take continuous values (e.g., for soft audio-driven conditioning). In such cases, the indicator $\mathbb{1}_{\{m_{i,j} > \tau\}}$ selects the time-steps where the target activation is sufficiently strong.

Increasing the attention magnitude without constraint can lead to overly diffuse spatial maps (Qi et al. 2025), especially in multi-object scenes, which degrades the visual grounding of word tokens. To regularize this behavior and preserve spatial consistency, we introduce additional loss terms in the following paragraph.

Entropy regularization. Word-level attention is typically spatially focused rather than dispersed (see Figure 2). To discourage excessive spreading of attention during optimization, we regularize the entropy of the spatial attention maps. Specifically, we apply this regularization only at temporal indices where the word is expected to be active (i.e., $m_{i,j} > \tau$), resulting in:

$$\mathcal{L}_{\text{entropy}}^t = \frac{1}{T'} \sum_{j=1}^{T'} \mathbb{1}_{[m_{i,j} > \tau]} \cdot \mathcal{H}(\bar{A}_{j,i}^t). \quad (8)$$

Here, $\mathcal{H}(\bar{A})$ denotes the Shannon entropy computed over the spatial dimensions.

Spatial consistency penalty. To maintain spatial consistency, we penalize deviations between the initial and optimized spatial attention maps for the target word. Here, $\hat{A}_{j,i}^t$

denotes the spatial attention map before optimization at step t , for word i at frame j . The penalty is defined as

$$\mathcal{L}_{\text{spatial}}^t = \left\| \sum_{j=1}^{T'} \left(\hat{A}_{j,i}^t - \bar{A}_{j,i}^t \right) \right\|_2^2, \quad (9)$$

where the difference is computed over the spatial dimensions, after summing across all latent frames.

Full objective. The combined loss at step t is:

$$\mathcal{L}^t = \mathcal{L}_{\text{corr}}^t + \lambda_1 \mathcal{L}_{\text{energy}}^t + \lambda_2 \mathcal{L}_{\text{entropy}}^t + \lambda_3 \mathcal{L}_{\text{spatial}}^t, \quad (10)$$

where $\lambda_1, \lambda_2, \lambda_3$ are hyperparameters used to calibrate the contribution of the regularization terms. This objective is optimized over latent codes during inference; model weights remain fixed.

Correlation-based early stopping. Some videos naturally align more closely with the temporal objective and therefore require fewer optimization steps. To adaptively allocate compute, we introduce a stopping rule based on the Pearson correlation in the temporal loss $\mathcal{L}_{\text{corr}}^t$. Specifically, for each denoising step t , we perform up to l optimization iterations. If the correlation exceeds a threshold τ_{corr} , we terminate optimization early for that step; otherwise, we continue refining until the limit is reached.

5 Experiments

Below, we describe the applications and evaluation protocols used in our experiments.

Setup. We use Wan 2.1 1.3B as our text-to-video backbone. All experiments were run on a single NVIDIA H200 GPU. TEMPOCONTROL takes approximately ~ 460 s per video, compared to ~ 170 s for vanilla generation. Hyperparameter details and ablations are available in the appendix.

Baseline. We employ Wan 2.1 1.3B with explicit temporal cues in the prompt (e.g., “...at the third second...”). We describe the exact phrasing details in the appendix.

Metrics. We evaluate on VBench (Huang et al. 2024), reporting temporal-related metrics: Subject Consistency (main subject coherence across frames), Background Consistency (background stability), Motion Smoothness (absence of temporal flicker), and Dynamic Degree (overall motion magnitude), as well as quality metrics: Aesthetic Quality (visual appeal) and Imaging Quality (clarity of frames). Additional details about these metrics are provided in the appendix.

We also introduce a new metric, Temporal Accuracy, which measures whether objects appear in the correct frames as specified by the prompt, and provides breakdowns for both object absence and presence. By default, the official VBench metric uses the GReT detector (Wu et al. 2024). To provide a more up-to-date assessment, we report temporal accuracy results using YOLOv10 (Wang et al. 2024a).

For movement, Temporal Accuracy is assessed by matching the movement time specified in the prompt with the second exhibiting the most movement, as determined by optical

Method	Temporal Accuracy	T. Absence Accuracy	T. Presence Accuracy	Subject Consistency	Background Consistency	Motion Smoothness	Dynamic Degree	Aesthetic Quality	Imaging Quality
One Object									
Text	63.94%	67.38%	60.50%	84.66%	92.30%	99.16%	47.50%	45.98%	53.76%
Ours	81.00%	88.75%	72.91%	80.60%	90.33%	99.05%	38.75%	44.37%	52.99%
Two Objects									
Text	37.50%	45.85%	29.15%	92.06%	95.32%	98.92%	62.20%	53.26%	68.56%
Ours	55.00%	66.46%	43.54%	92.21%	95.43%	99.19%	41.46%	56.55%	70.66%
Movement									
Text	19%	–	–	93.17%	95.91%	98.10%	73.00%	55.81%	60.46%
Ours	53%	–	–	92.86%	95.67%	98.20%	80.00%	55.06%	61.76%

Table 1: Comparison against Wan 2.1 across three temporal-control applications: (i) one object, (ii) two objects, and (iii) movement. Results for irrelevant metrics are marked with –. Higher values indicate better performance for all metrics.

Method	Multiple Object (GriT)	Multiple Object (YOLO)	Dynamic Degree
Text	74.13%	61.54%	30.49%
Ours	76.37%	65.73%	18.78%

Table 2: Multiple object benchmark assessing the ability to depict multiple objects across the video.

Question Type	Ours	Baseline	Same
Temporal Accuracy	61.51%	16.94%	21.55%
Visual Quality	62.66%	25.99%	11.35%

Table 3: User study results for temporal accuracy and visual quality.

flow. Each video is sampled at 4 frames per second; we compute the average flow magnitude per second, and the second with the highest average is considered the most active.

5.1 Quantitative Results

Single object temporal control. In Table 1 (One Object), our method improves temporal accuracy by 17.06% to 81.00%, with similar gains in temporal absence (+21.37) and presence (+12.41) accuracy compared to text prompts with explicit time cues. Image Quality and Aesthetic Quality remain comparable, with a difference of 1%.

We observe decreases in Dynamic Degree, dropping by 8.75% to 38.75%, reflecting reduced dynamics due to temporal control, which requires object presence over extended periods of the video.

Two objects temporal control. In Table 1 (Two Objects), we show that the two-object setting presents a significant challenge, with the baseline achieving only 37.5% temporal accuracy. Our method improves to 55.0%. Temporal absence and presence accuracies also show gains of 20.6% and 14.4%, respectively. Imaging and Aesthetic Quality increase by about 2% each. Subject Consistency, Background

Consistency, and Motion Smoothness remain similar between methods. At the same time, we find that Dynamic Degree is reduced here, as in the one-object case, by roughly 21%. This reflects the trade-off imposed by temporal control, which requires static background objects and reduces dynamic content.

Movement temporal control. Table 1 (Movement) shows that TEMPOCONTROL significantly improves temporal accuracy (53% vs. 19%) compared to the text-prompt baseline. We note that the original temporal accuracy of the model is similar to random, indicating that Wan 2.1 does not capture movement cues at all. The Dynamic Degree here increases, as the goal is to introduce more movement, demonstrating that our approach successfully creates more pronounced motion. Imaging and Aesthetic Quality remain on par with the baseline. Overall, our explicit temporal guidance sharpens movement timing without compromising visual quality and consistency.

Multiple objects benchmark. We also report results on the VBench Multiple Objects benchmark in Table 2, which tests the ability to generate two objects described in the input text throughout the entire video. We observe improved performance on the Multiple Object metric (76.34% vs. 74.13%), although this comes at the cost of reduced video dynamics. Detailed results are provided in the appendix.

Human evaluation. We conducted a human evaluation with 50 annotators, each comparing 16 videos (8 one-object, 8 two-object) generated by TEMPOCONTROL and Wan 2.1. Annotators selected which video was better in terms of temporal accuracy and visual quality, or if they were the same. As shown in Table 3, our method outperformed the baseline in temporal accuracy (61.51% vs. 16.94%) and also improved visual quality. For temporal accuracy, 21.55% of responses indicated no preference, likely due to subtle timing differences. Full details of the evaluation are provided in the appendix.



Figure 4: Examples of videos generated by Wan 2.1 (left) and our method with temporal conditioning (right) for prompts that specify temporal conditions. The prompts are simplified for brevity. We show frames corresponding to the first, middle, and last third of each video.

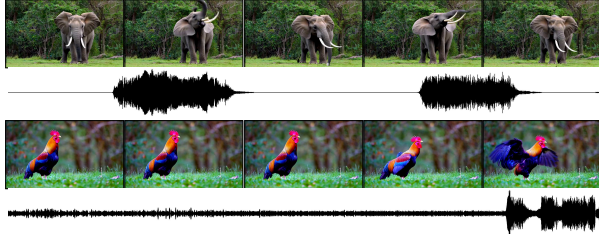


Figure 5: Examples of video alignment to an audio signal.

5.2 Qualitative Results

In Figure 4, we show four videos generated to depict objects or actions at specific times. In the first row, where a single apple is expected to appear at the fourth second, Wan 2.1 generates the apple near the middle of the five-second video, while our method correctly places it near the end of the video. For the “cat and dog, dog at first half” prompt, Wan 2.1 fails to show the dog at the beginning of the video, whereas our approach accurately places the dog in the first half. In the “magician pulling a rabbit last second” scenario, Wan 2.1 displays the rabbit from the start, instead of only in the final second as required. Similarly, for “tiger leaping first second,” Wan 2.1 does not capture the leaping motion at the correct time, while our method, with temporal conditioning, accurately generates the requested action. All videos are included in the supplementary material.

5.3 Audio-Visual Alignment

We also experimented with zero-shot alignment of video to external audio by using a preprocessed audio envelope as the temporal condition. Given a waveform y , we extract its onset strength envelope s_t , adaptively pool it to match the number of frames, and normalize to $[0, 1]$ via min-max normalization. Prominent peaks are preserved via thresholding

and Gaussian smoothing:

$$\tilde{s}_t = \begin{cases} \hat{s}_t, & \text{if } \hat{s}_t \geq \tau_{\text{audio}}, \\ \text{GaussianSmooth}(\hat{s}_t; \sigma), & \text{otherwise.} \end{cases} \quad (11)$$

where τ_{audio} is a threshold for peak preservation, and σ is the standard deviation of the Gaussian kernel used for smoothing.

In Figure 5, we present examples of accurate video adaptation to audio peaks, with additional results in the appendix. Although experiments are limited to simple cases with prominent peaks, these findings suggest a promising direction for aligning generated video with audio without requiring costly training on curated datasets.

5.4 Discussions

Text temporal control limitations. In our experiments, adding explicit timing to Wan 2.1 prompts did not improve temporal accuracy and often reduced video and image quality. For example, temporal accuracy fell from 65% to 64%, and video quality from 56% to 53%. For fairness, all reported results use the same prompt setup as the text baseline, despite omitting explicit timing, which yields higher performance for our approach. For instance, for a single object, we observe a video quality of 56% compared to 53%, with the same temporal accuracy of 81%. See the appendix for details.

Consistency limitations. Temporal conditioning may lead to perceptual changes in background or unspecified features. For example, it can alter the color of a cat (see Figure 1). Although perceptual consistency is often preserved, our current objectives do not fully guarantee it, which remains a promising area for future work.

5.5 Conclusions

Current text-to-video models generate semantically accurate and high-quality videos, but they lack precise control over

the temporal appearance of objects and actions. Our results show that existing text-conditioning approaches are insufficient for temporal control. To address this gap, we present a data-free temporal conditioning technique, which maintains video quality while enabling fine-grained temporal control through attention steering. We hope our approach will inspire new solutions to tasks such as audio-video alignment, as discussed in this work.

References

Avrahami, O.; Patashnik, O.; Fried, O.; Nemchinov, E.; Aberman, K.; Lischinski, D.; and Cohen-Or, D. 2025. Stable flow: Vital layers for training-free image editing. In *Proceedings of the Computer Vision and Pattern Recognition Conference*, 7877–7888.

Bar-Tal, O.; Chefer, H.; Tov, O.; Herrmann, C.; Paiss, R.; Zada, S.; Ephrat, A.; Hur, J.; Liu, G.; Raj, A.; et al. 2024. Lumiere: A space-time diffusion model for video generation. In *SIGGRAPH Asia 2024 Conference Papers*, 1–11.

Battash, B.; Rozner, A.; Wolf, L.; and Lindenbaum, O. 2024. Obtaining favorable layouts for multiple object generation. *arXiv preprint arXiv:2405.00791*.

Battash, B.; Wolf, L.; and Lindenbaum, O. 2024. Revisiting the noise model of stochastic gradient descent. In *International Conference on Artificial Intelligence and Statistics*, 4780–4788. PMLR.

Blattmann, A.; Rombach, R.; Ling, H.; Dockhorn, T.; Kim, S. W.; Fidler, S.; and Kreis, K. 2023. Align your Latents: High-Resolution Video Synthesis with Latent Diffusion Models. In *Proceedings of the IEEE/CVF Conference on Computer Vision and Pattern Recognition*, 22563–22575.

Chefer, H.; Alaluf, Y.; Vinker, Y.; Wolf, L.; and Cohen-Or, D. 2023. Attend-and-excite: Attention-based semantic guidance for text-to-image diffusion models. *ACM transactions on Graphics (TOG)*, 42(4): 1–10.

Dahary, O.; Patashnik, O.; Aberman, K.; and Cohen-Or, D. 2024. Be yourself: Bounded attention for multi-subject text-to-image generation. In *European Conference on Computer Vision*, 432–448. Springer.

Feng, W.; Liu, C.; Liu, S.; Wang, W. Y.; Vahdat, A.; and Nie, W. 2025. BlobGEN-Vid: Compositional Text-to-Video Generation with Blob Video Representations. *arXiv:2501.07647*.

Geng, D.; Herrmann, C.; Hur, J.; Cole, F.; Zhang, S.; Pfaff, T.; Lopez-Guevara, T.; Aytar, Y.; Rubinstein, M.; Sun, C.; et al. 2025. Motion prompting: Controlling video generation with motion trajectories. In *Proceedings of the Computer Vision and Pattern Recognition Conference*, 1–12.

Gupta, A.; Yu, L.; Sohn, K.; Gu, X.; Hahn, M.; Li, F.-F.; Essa, I.; Jiang, L.; and Lezama, J. 2024. Photorealistic video generation with diffusion models. In *European Conference on Computer Vision*, 393–411. Springer.

He, H.; Xu, Y.; Guo, Y.; Wetzstein, G.; Dai, B.; Li, H.; and Yang, C. 2024. CameraCtrl: Enabling Camera Control for Text-to-Video Generation. *arXiv:2404.02101*.

Hertz, A.; Mokady, R.; Tenenbaum, J.; Aberman, K.; Pritch, Y.; and Cohen-Or, D. 2023. Prompt-to-Prompt Image Editing with Cross-Attention Control. In *The Eleventh International Conference on Learning Representations*.

Huang, Z.; He, Y.; Yu, J.; Zhang, F.; Si, C.; Jiang, Y.; Zhang, Y.; Wu, T.; Jin, Q.; Champaisit, N.; et al. 2024. Vbench: Comprehensive benchmark suite for video generative models. In *Proceedings of the IEEE/CVF Conference on Computer Vision and Pattern Recognition*, 21807–21818.

Li, J.; Yu, S.; Lin, H.; Cho, J.; Yoon, J.; and Bansal, M. 2025. Training-free Guidance in Text-to-Video Generation via Multimodal Planning and Structured Noise Initialization. *arXiv preprint arXiv:2504.08641*.

Lian, L.; Shi, B.; Yala, A.; Darrell, T.; and Li, B. 2023. Llm-grounded video diffusion models. *arXiv preprint arXiv:2309.17444*.

Qi, J.; Liu, J.; Tang, H.; and Zhu, Z. 2025. Beyond semantics: Rediscovering spatial awareness in vision-language models. *arXiv preprint arXiv:2503.17349*.

Shaulov, A.; Hazan, I.; Wolf, L.; and Chefer, H. 2025. FlowMo: Variance-Based Flow Guidance for Coherent Motion in Video Generation. *arXiv preprint arXiv:2506.01144*.

Singer, U.; Polyak, A.; Hayes, T.; Yin, X.; An, J.; Zhang, S.; Hu, Q.; Yang, H.; Ashual, O.; Gafni, O.; et al. 2022. Make-A-Video: Text-to-Video Generation without Text-Video Data. *arXiv preprint arXiv:2209.14792*.

Wan, T.; Wang, A.; Ai, B.; Wen, B.; Mao, C.; Xie, C.-W.; Chen, D.; Yu, F.; Zhao, H.; Yang, J.; et al. 2025. Wan: Open and advanced large-scale video generative models. *arXiv preprint arXiv:2503.20314*.

Wang, A.; Chen, H.; Liu, L.; Chen, K.; Lin, Z.; Han, J.; et al. 2024a. Yolov10: Real-time end-to-end object detection. *Advances in Neural Information Processing Systems*, 37: 107984–108011.

Wang, J.; Zhang, Y.; Zou, J.; Zeng, Y.; Wei, G.; Yuan, L.; and Li, H. 2024b. Boximator: Generating rich and controllable motions for video synthesis. *arXiv preprint arXiv:2402.01566*.

Wei, M.; Yu, C.; Zhou, J.; and Wang, F. 2025. 3DV-TON: Textured 3D-Guided Consistent Video Try-on via Diffusion Models. *arXiv preprint arXiv:2504.17414*.

Wu, J.; Wang, J.; Yang, Z.; Gan, Z.; Liu, Z.; Yuan, J.; and Wang, L. 2024. Grit: A generative region-to-text transformer for object understanding. In *European Conference on Computer Vision*, 207–224. Springer.

Yang, Z.; Teng, J.; Zheng, W.; Ding, M.; Huang, S.; Xu, J.; Yang, Y.; Hong, W.; Zhang, X.; Feng, G.; et al. 2024. Cogvideox: Text-to-video diffusion models with an expert transformer. *arXiv preprint arXiv:2408.06072*.

Supplementary Material: TEMPOCONTROL – Temporal Attention Guidance for Text-to-Video Models

This supplementary material provides detailed information supporting our main paper. It includes algorithmic implementation, experimental design, application-specific configurations, extended quantitative and qualitative results, and a human evaluation setup. Videos and code are provided as part of the supplementary materials package.

Specifically, we include:

1. Full algorithm and pseudocode (Section .1).
2. Experimental setup and hyperparameters (Section .2).
3. Configuration details for each application setting (Section .3).
4. Human evaluation protocol and interface (Section .4).
5. Extended quantitative results for multi-object grounding (Section .5).
6. Ablation study of loss components and qualitative failure modes (Section .6).
7. Analysis of prompt phrasing and its impact on performance (Section .7).
8. Additional qualitative results with sampled frames (Section .8).

.1 Algorithm Pseudo-code

Algorithm 1 outlines our inference-time optimization procedure. Starting from noise z_T , we iteratively steer the latent code during the first k denoising steps of the diffusion process. At each step t , we compute cross-attention maps from the video-text model DiT and derive the scalar temporal attention a_i^t for each token p_i .

The optimization loss \mathcal{L} combines four components: correlation alignment \mathcal{L}_c^t , energy modulation $\mathcal{L}_{\text{enr}}^t$, entropy regularization $\mathcal{L}_{\text{ent}}^t$, and spatial consistency \mathcal{L}_s^t . The latent code is updated via gradient descent for up to l steps per denoising timestep, or until the Pearson correlation exceeds a threshold τ_{corr} . After optimization, the standard denoising process resumes to produce the final latent z_0 .

Algorithm 1: TEMPOCONTROL: Temporal Attention-Guided Inference-Time Steering

Input: Prompt \mathcal{P} , tokens p_i with temporal masks m_i , total diffusion steps T , optimized steps k , max updates per step l , correlation threshold τ_{corr} , model DiT

Output: Final latent z_0

```

1: Initialize  $z_T \sim \mathcal{N}(0, I)$ 
2: for  $t = T, T-1, \dots, T-k+1$  do
3:   for  $u = 1$  to  $l$  do
4:     Extract cross-attentions  $A^t$  from DiT( $z_t, \mathcal{P}, t$ )
5:     Average heads and layers:  $\bar{A}^t$ 
6:      $\mathcal{L} \leftarrow 0$ 
7:     for each  $p_i$  with  $m_i$  do
8:        $a_i^t \leftarrow [\langle \bar{A}_{j,i}^t \rangle_{x,y}]_{j=1}^{T'}$ 
9:        $\mathcal{L}_c^t \leftarrow -\text{Corr}(m_i, \text{minmax}(a_i^t))$ 
10:       $\mathcal{L}_\oplus^t \leftarrow \frac{1}{T'} \sum_{j=1}^{T'} \mathbb{1}[m_{i,j} > \tau] \cdot a_{i,j}^t$ 
11:       $\mathcal{L}_\ominus^t \leftarrow \frac{1}{T'} \sum_{j=1}^{T'} \mathbb{1}[m_{i,j} \leq \tau] \cdot a_{i,j}^t$ 
12:       $\mathcal{L}_{\text{enr}}^t \leftarrow \mathcal{L}_\ominus^t - \mathcal{L}_\oplus^t$ 
13:       $\mathcal{L}_{\text{ent}}^t \leftarrow \frac{1}{T'} \sum_{j=1}^{T'} \mathbb{1}[m_{i,j} > \tau] \cdot \mathcal{H}(\bar{A}_{j,i}^t)$ 
14:       $\mathcal{L}_s^t \leftarrow \sum_{j=1}^{T'} \|\bar{A}_{j,i}^t - \bar{A}_{j,i}^t\|_2^2$ 
15:       $\mathcal{L} \leftarrow \mathcal{L} + \mathcal{L}_c^t + \lambda_1 \mathcal{L}_{\text{enr}}^t + \lambda_2 \mathcal{L}_{\text{ent}}^t + \lambda_3 \mathcal{L}_s^t$ 
16:    end for
17:     $z'_t \leftarrow z_t - \alpha_t \nabla_{z_t} (\mathcal{L}/N)$ 
18:    if All  $\mathcal{L}_{\text{corr}}^t \leq \tau_{\text{corr}}$  then
19:      break
20:    end if
21:     $z_t \leftarrow z'_t$ 
22:  end for
23:   $z_{t-1} \leftarrow \text{DiT}(z'_t, \mathcal{P}, t)$ 
24: end for
25: Continue denoising using the standard denoising diffusion process for  $t = T-k, \dots, 1$ 
26: return  $z_0$ 

```

2 Experimental Setup

Hyperparameters were tuned early using a small validation set specific to each task. While large-scale ablations were limited by computational constraints, we found the method to be robust across scenarios with only minor adjustments.

All experiments are conducted using `Wan 2.1` as the backbone. We apply a classifier-free guidance scale of 6 and a sample shift of 3 during generation.

For single-object scenes, we use $\lambda_1=1$, $\lambda_2=10$, $\lambda_3=1$, a learning rate of 0.0005, a Pearson stopping threshold of $\tau_{\text{corr}}=0.9$, and apply optimization for the first $l=10$ denoising steps with up to $k=10$ gradient updates per step.

In two-object scenes, which require more aggressive guidance, we raise the learning rate to 0.001 for improved convergence. For motion-centric prompts, we reduce the temporal alignment weight to $\lambda_1=0.3$ and relax the Pearson threshold to $\tau_{\text{corr}}=0.85$ to allow more flexible optimization.

3 Applications Setup

Single-Object Temporal Control. To assess temporal grounding for individual objects, we construct a dataset using the 80 object categories detectable by the YOLO detector. These span common classes, such as animals and vehicles, as well as specific items, including handbags and sports equipment. Videos are generated from prompts of the form: “*An empty scene. Suddenly, $\langle o_1 \rangle$ appears out of nowhere, drawing all attention.*” Object classes are uniformly distributed across different time intervals.

Two-Object Temporal Control. We evaluate TEMPOCONTROL on 82 object pairs from the VBench protocol. Prompts take the form: “*The video begins with a serene view centered on $\langle o_1 \rangle$, with no sign of $\langle o_2 \rangle$. In the second half, $\langle o_2 \rangle$ unexpectedly appears, altering the dynamic of the scene.*” A static control signal (all ones) is used for $\langle o_1 \rangle$. We sample 20 evenly spaced frames and require $\langle o_1 \rangle$ to always be present. A frame is counted as successful if both objects are detected when $\langle o_2 \rangle$ is active, and only $\langle o_1 \rangle$ is detected when $\langle o_2 \rangle$ is inactive.

Motion Temporal Control. To test fine-grained temporal modulation of actions, we generate 100 videos using prompts such as: “*A video of $\langle s \rangle \langle v \rangle \langle a \rangle$ with a strong movement at the $\langle t \rangle$ second,*” where $\langle s \rangle$, $\langle v \rangle$, $\langle a \rangle$, and $\langle t \rangle$ denote subject, verb, adverb, and time reference, respectively. Example: “*A child jumping joyfully at the third second.*” The verb is controlled via a binary temporal mask (1 only at $\langle t \rangle$), while the subject is always present.

Multi-Object Accuracy. We benchmark TEMPOCONTROL on the VBench Multiple Objects benchmark, which evaluates the generation of all the mentioned objects. Each video is sampled at 16 evenly spaced frames. A frame is successful if both target objects are detected. The final score is the average per-frame success rate across all videos. We use all-one control signals for both objects and optimize only the first 4 denoising steps, skipping the Pearson-based stopping criterion.

.4 Human Evaluation Protocol

To assess temporal alignment and visual quality, we conducted a human preference study using side-by-side video comparisons. For each prompt, two videos were presented, one generated by our method and one by the text baseline, randomly assigned as Video A or B to avoid bias.

Annotators were asked to read the prompt and answer two questions: (1) Which video is more temporally accurate (i.e., does the object appear at the correct time and remain visible)? and (2) Which video looks more visually appealing? A “Same (Use sparingly!)” option was available if no difference was perceived.

Example screenshots of the evaluation interface are shown in Figures 6 and 7.

User Study- Temporal Control for Text to Video Diffusion Models

Welcome, and thank you very much for your willingness to participate!

This study is part of an academic research project and will take no more than a few minutes of your time.

The goal is to evaluate how well text-to-video diffusion models can generate **temporally accurate** videos. That is, whether objects appear at the exact time specified in the prompt.

Here's how it works:

You'll be shown **two videos at a time**, both generated from the **same prompt**.

Each prompt includes a **temporal instruction**, such as:

“A dog appears in the third second,” or “In the second half, a bottle appears.”

For each video pair, please answer two questions:

- **Which video is more temporally accurate?** (Does the object appear at the right time, and remain visible until the end of the video?)
- **Which video looks more visually appealing to you?** (This includes overall quality, consistency, and how much sense the video makes.)

Your answers will help us compare a baseline model with our new method.

Thanks again, and enjoy the mini tour into the world of text-to-video models :)

Figure 6: Evaluation interface showing the prompt and two videos (A and B) for comparison.

Prompt:

"The video begins with a serene view centered on the **bicycle**, with no sign of the **truck**. In the **second half**, the **truck** unexpectedly appears, altering the dynamic of the scene"

Video A



Video B



2.

Which video is more temporally accurate?

(Does the object appear at the right time, and remain visible until the end of the video?)

*

- Video A
- Video B
- Same (Use sparingly!)

2.

*

Which video looks more visually appealing to you?

- Video A
- Video B
- Same (Use sparingly!)

Figure 7: Second example of the human evaluation interface.

.5 Multi-Object Evaluation

We report extended results on multi-object text-to-video generation using the VC-Bench benchmark. In this setting, prompts reference multiple entities with temporal conditions (e.g., “A dog in the beginning, then a cat”). We compare our method against a text baseline.

Table 4 summarizes results. Our method achieves substantial gains in object-centric metrics. Specifically, we improve multi-object accuracy from 74.1% to 76.4% (GriT) and from 61.5% to 65.7% (YOLO), demonstrating improved temporal grounding and visibility of both entities. We also observe improvements across all consistency metrics, including subject consistency (from 97.2% to 97.8%) and background consistency (from 97.6% to 98.1%).

The dynamic degree shows a slight reduction (from 30.5% to 18.8%), which reflects a known tradeoff: our method promotes temporal consistency, often leading to more stable object appearance throughout the video. As a result, motion may be reduced.

However, we note a limitation of this metric: VC-Bench implicitly favors videos where objects are present in all frames. A more suitable benchmark might instead reward appearances rather than requiring full-video presence.

Table 4: Full results for Multiple object benchmark results. Best results per column are in bold.

Method	Multiple Object (GriT)	Multiple Object (YOLO)	Subject Consistency	Background Consistency	Motion Smoothness	Dynamic Degree	Aesthetic Quality	Imaging Quality
Text	74.13%	61.54%	97.22%	97.56%	99.18%	30.49%	62.84%	70.25%
Ours	76.37%	65.73%	97.81%	98.10%	99.40%	18.78%	62.52%	70.21%

.6 Ablations

Table 5 presents an ablation study in the two-object setting, evaluating the impact of removing the energy term, entropy term, and spatial penalty.

Omitting the energy term results in a modest decrease in temporal accuracy (from 55% to 52.56%). In contrast, removing the entropy term has a more significant effect: temporal accuracy falls to 48.96%, and the temporal presence accuracy drops sharply from 43.54% to 34.76%. Subject Consistency, Aesthetic Quality, and Imaging Quality also decline. Without entropy regularization, attention becomes overly diffuse, often blending the two objects.

Qualitative analysis shows that without the entropy term, the model frequently replaces the static object with the dynamic one (see Section .3 for details on the static and temporally conditioned objects, and Figure 8 for qualitative results).

Table 5: Ablation results for the two-object setting.

Method	Temporal Accuracy	T. Absence Accuracy	T. Presence Accuracy	Subject Consistency	Background Consistency	Motion Smoothness	Dynamic Degree	Aesthetic Quality	Imaging Quality
Text baseline	37.50%	45.85%	29.15%	92.06%	95.32%	98.92%	62.20%	53.26%	68.56%
Ours	55.00%	66.46%	43.54%	92.21%	95.43%	99.19%	41.46%	56.55%	70.66%
No energy	52.56%	58.90%	46.22%	92.31%	95.45%	99.34%	46.34%	56.12%	71.15%
No entropy	48.96%	63.17%	34.76%	89.99%	94.39%	98.92%	53.66%	54.66%	68.95%
No spatial	52.01%	60.85%	43.17%	92.76%	95.67%	99.23%	48.78%	56.75%	70.25%

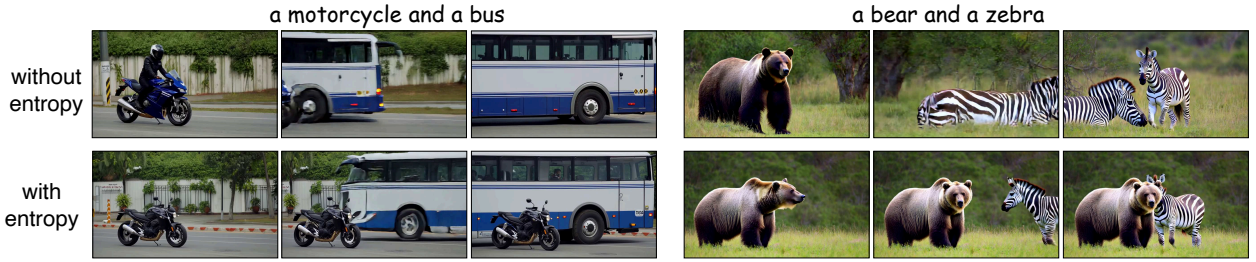


Figure 8: Ablation study. Left: without entropy regularization, the motorcycle disappears. Right: the bear is incorrectly replaced by a zebra.

.7 Impact of Temporal Phrasing

We analyze the effect of using explicit temporal phrasing (e.g., “in the third second,” “in the second part of the video”) in the prompt for the one-object setup. Table 6 compares Wan 2.1 and our method, each evaluated with and without such phrasing.

For Wan 2.1, omitting temporal cues slightly improves temporal accuracy (63.94% to 65.18%) and yields higher aesthetic (45.98% to 48.78%) and imaging quality (53.76% to 59.99%), suggesting that the model struggles to interpret or apply explicit timing effectively.

Our method benefits even more: removing temporal phrases results in the highest temporal accuracy (81.12%) along with gains in aesthetic (48.16%) and imaging quality (56.32%). We hypothesize that Wan 2.1 is not trained to handle precise temporal expressions, and current attention mechanisms may not effectively capture their semantics. As a result, such phrasing introduces ambiguity. In contrast, concise prompts without explicit timing allow our method to align more reliably with the intended temporal structure.

For fairness, all main paper results use prompts with temporal phrasing to match the baseline. However, these findings suggest that our method achieves even stronger performance when using simpler prompts without explicit timing constraints.

Table 6: Effect of temporal phrasing in prompts for the one-object setup. Removing explicit timing improves video quality.

Method	Temp. Acc.	T. Abs. Acc.	T. Pres. Acc.	Subj. Cons.	Backg. Cons.	Motion Smooth.	Dyn. Deg.	Aesthetic	Imaging
Wan with time	63.94%	67.38%	60.50%	84.66%	92.30%	99.16%	47.50%	45.98%	53.76%
Wan without time	65.18%	65.12%	65.25%	85.29%	92.44%	99.22%	45.00%	48.78%	59.99%
Ours with time	81.00%	88.75%	72.91%	80.60%	90.33%	99.05%	38.75%	44.37%	52.99%
Ours without time	81.12%	84.75%	77.50%	81.29%	90.72%	99.06%	35.00%	48.16%	56.32%

.8 Additional Qualitative Examples

We provide qualitative results across the one-object, two-object, and motion-based setups. For each example, we show sampled frames from the generated videos, illustrating the temporal grounding of object appearances. Prompts are abbreviated for brevity, indicating the key object and its expected time of appearance. Note that once introduced, the object is expected to persist until the end of the video. **Videos can be viewed on the project page.**



Text

Ours

apple 4sec



Text

Ours

bear 3sec



Text

Ours

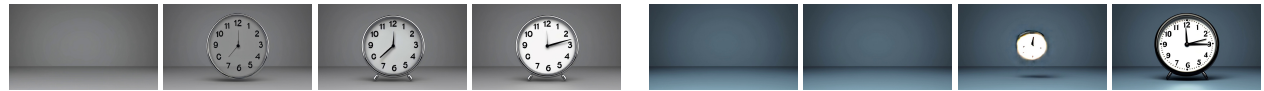
bench 2sec



Text

Ours

bus 2sec



Text

Ours

clock 5sec



Text

Ours

elephant 3sec



Text

Ours

surfboard 3sec



Text

Ours

tie 3sec

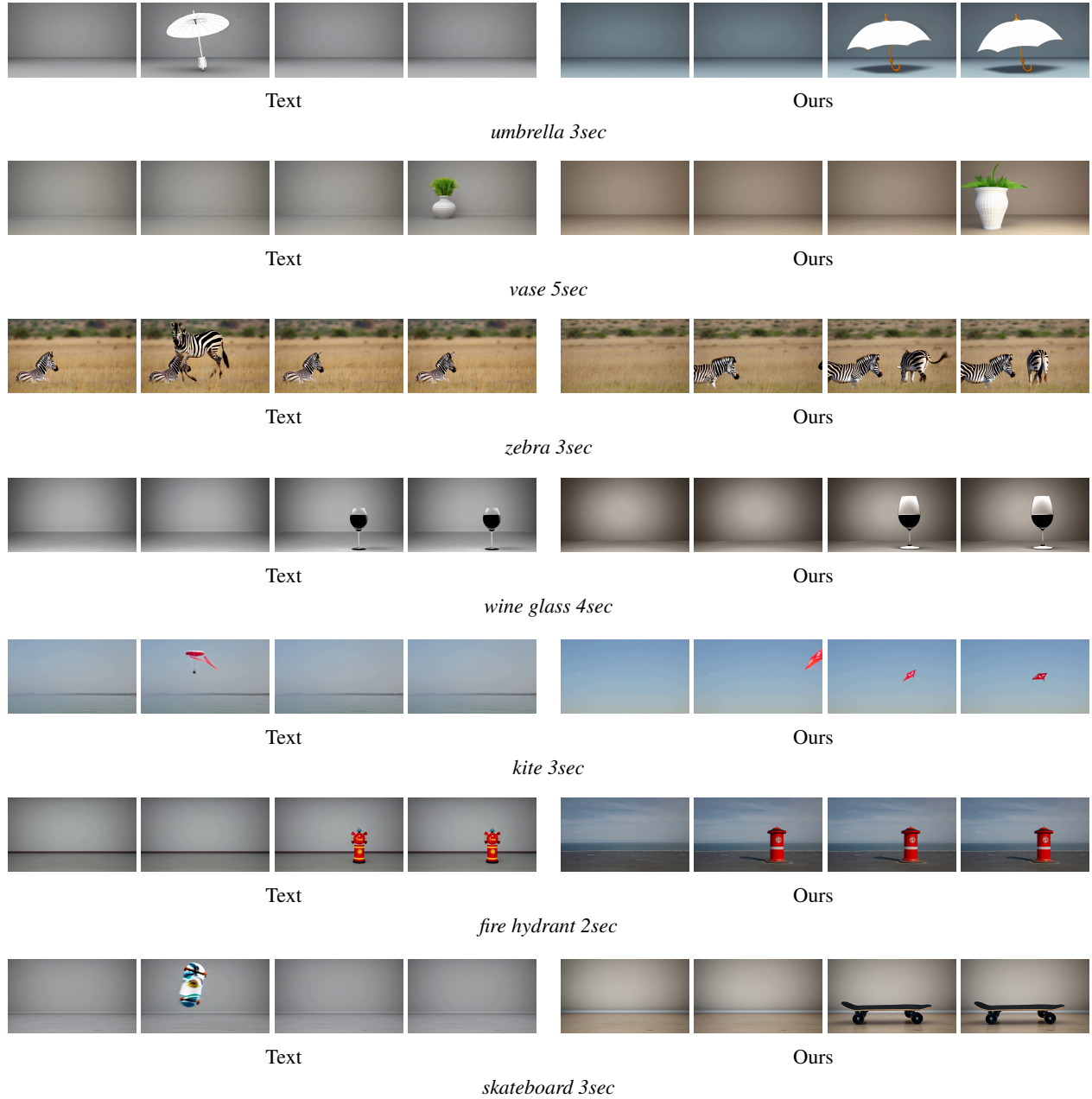


Figure 9: One object Text vs Ours.



Text

Ours

a bird and a cat



Text

Ours

a boat and an airplane



Text

Ours

a book and a clock



Text

Ours

a carrot and an umbrella



Text

Ours

a chair and a couch



Text

Ours

a giraffe and a bird



Text

Ours

a horse and a sheep



Text

Ours

a teddy bear and a frisbee

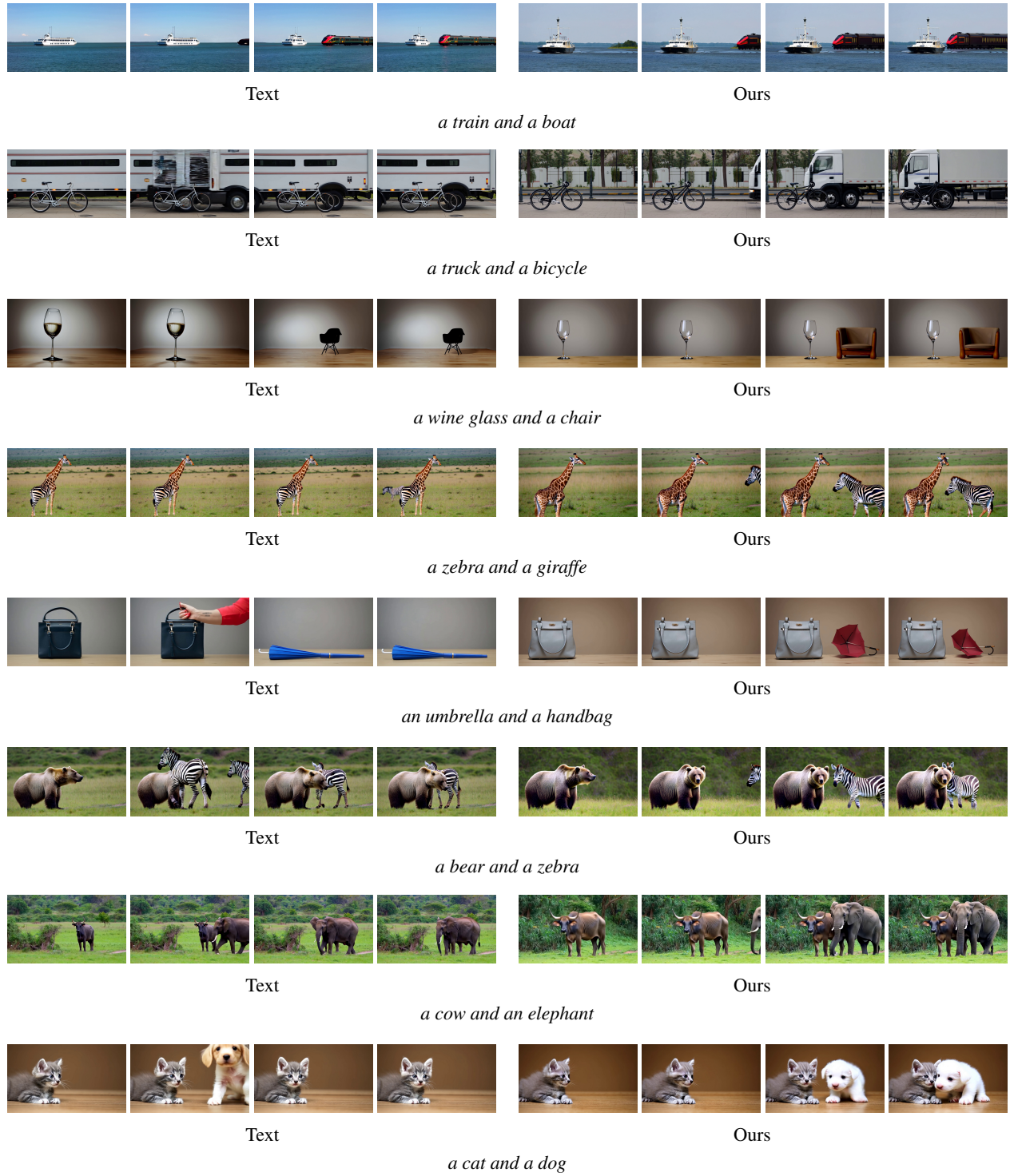


Figure 10: Two objects Text vs Ours.



Text

Ours

chimpanze clapping 1sec



Text

Ours

horse shaking its mane 4sec



Text

Ours

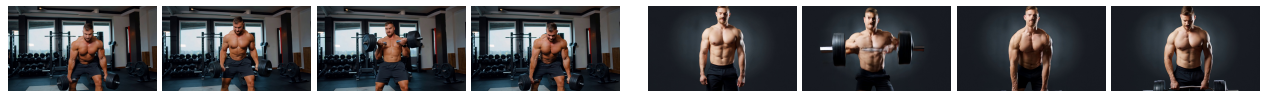
lion roaring 1sec



Text

Ours

magician pulling rabbit 5sec



Text

Ours

man lifting weights 3sec



Text

Ours

rabbit thumping 4second



Text

Ours

snake slithering 1sec



Text

Ours

tiger leaping 1sec



Text

Ours

child jumping 1sec



Text

Ours

wolf howling 2sec

Figure 11: Movement Text vs Ours.